Physica B 497 (2016) 86–92

Contents lists available at ScienceDirect

Physica B

journal homepage: www.elsevier.com/locate/physb

Effect of deep native defects on ultrasound propagation in $TlInS_2$ layered crystal

MirHasan Yu. Seyidov [a,b,*], Rauf A. Suleymanov [a,b], Andrei P. Odrinsky [c], Cafer Kırbaş [a,d]

[a] Department of Physics, Gebze Technical University, 41400 Gebze, Kocaeli, Turkey
[b] Institute of Physics of NAS of Azerbaijan, H. Javid Avenue, 33, AZ-1143 Baku, Azerbaijan
[c] Institute of Technical Acoustics, National Academy of Sciences of Belarus, Lyudnikov Avenue 13, Vitebsk 210717, Belarus
[d] The Scientific and Technological Research Council of Turkey, National Metrology Institute (TUBITAK UME), PQ 54 41470 Gebze, Kocaeli, Turkey

ARTICLE INFO

Article history:
Received 27 May 2016
Received in revised form
13 June 2016
Accepted 14 June 2016
Available online 16 June 2016

Keywords:
Ferroelectric–semiconductors
Photo-induced current transient spectroscopy
Pulse-echo method
Deep level defects
Velocity of longitudinal and transverse ultrasonic waves

ABSTRACT

We have investigated *p*-type semiconductor–ferroelectric $TlInS_2$ by means of Photo-Induced Current Transient Spectroscopy (PICTS) technique in the temperature range 77–350 K for the detection of native deep defect levels in $TlInS_2$. Five native deep defect levels were detected and their energy levels and capture cross sections were evaluated. Focusing on these data, the influence of these defects on the longitudinal and transverse ultrasound waves propagation as well as the effect of electric field on ultrasound waves were studied at different temperatures. The acoustic properties were investigated by the pulse-echo method. The direct contribution of thermally activated charged defects to the acoustic properties of $TlInS_2$ was demonstrated. The key role of charged native deep level defects in elastic properties of $TlInS_2$ was shown.

1. Introduction

$TlInS_2$ crystals have a layered crystalline structure and consist of separate layers with strong ion–covalent bonding between the atoms and weak van der Waals bonding between the layers. $TlInS_2$ usually has a p-type conductivity. Currently, *n*-type doping in $TlInS_2$ is still a daunting challenge. This has impeded the practical application of $TlInS_2$ in optoelectronic devices. The difficulty in doping of $TlInS_2$ is attributed to presence of some degree of disorder in material. Disorder is inherently present in the highly compensated semiconductors. A number of experimental properties of the as – grown $TlInS_2$ show that it is highly compensated semiconductor demonstrating the properties of amorphous materials [1,2].

The physical characterizations of compensated semiconductors depend upon the spatial electrostatic potential of the charged native deep level defects (donors and acceptors) contained inside the sample. The native deep levels in $TlInS_2$ layered semiconductor have not yet been fully characterized and understood, even though this material has been studied for many decades. Only a few results on investigations of traps in $TlInS_2$ have appeared so far in the literature [3–7]. Different methods have been available in practice to identify the deep level defects in the gap of this material. One of these methods is Deep Level Transient Spectroscopy (DLTS) but this method could fail to investigate the high resistance $TlInS_2$ semiconductor. Another well-known technique is Photo-induced Current Transient Spectroscopy (PICTS) and this method was selected to determine the traps in $TlInS_2$.

The other special issue related with crystals of $TlInS_2$ family is the extremely high sensitivity to external fields; electrical field, illumination, temperature annealing, etc. [8-10]. The only explanation that was put forward in our previous investigations was connected with the great role played of some defects characteristic for such crystals.

In this paper we try to make an interconnection between two problems outlined above investigating the defect structure and elastic properties of $TlInS_2$ crystals at the same time.

We present a detailed study of specially undoped $TlInS_2$ crystals using PICTS technique. The PICTS-technique has the special feature of detecting traps which may lay quite deep in the forbidden gap-a characteristics which other commonly used techniques (e.g., thermally stimulated current or luminescence techniques) do not possess. To our knowledge, this is the first use of this technique in the study of undoped $TlInS_2$. Several PICTS measurements have been carried out on Tb, Er, La and B doped $TlInS_2$

* Corresponding author at: Department of Physics, Gebze Technical University, Gebze 41400, Kocaeli, Turkey.
E-mail address: smirhasan@gtu.edu.tr (M.Yu. Seyidov).

http://dx.doi.org/10.1016/j.physb.2016.06.010
0921-4526/

with the aim to characterize the defects produced by dopand which in turn affects the polarization properties of crystal [11–15].

PICTS has become a widely used technique to determine the electronic properties of deep level traps in semiconductors. It yields the position of the energy level of a defect in the band gap, the capture cross section of this deep levels in high-resistivity materials. The principle of PICTS technique have been reported in numerous studies [16–25]. It is the variant of DLTS method [23,26], where the light excitation is employed the creation of defects filling by non-equilibrium charge carriers. In this technique, a voltage is applied between two ohmic contacts on the sample. Electron-hole pairs are generated in the entire depth (by choosing the appropriate wavelength of the light) of the sample by a light pulse. During this illumination period the defects (electron and hole traps) are filled by carriers generated by light, this process is called the filling process of the traps. Immediately after removal of the optical pulse at t=0, electrons and holes trapped in the defects emit and drift in the electric field when $t > 0$. The process is called the emission of the charge carriers from the traps. A rapid decrease in the current flowing through the sample owing to the recombination of free photocarriers is observed followed by a slower current transient owing to the thermally stimulated release of carriers from traps. This current transient is the source of the PICTS signal [16–25].

As a result, the investigation of electrical activity of defects in high-resistively or semi insulating materials is allowed. Under the study of semiconductors having ferroelectric properties it is important that light impulse with suitable photon energies can change the defects charge state without significant perturbation of crystal domain structure. The last case take place under applying the conventional DLTS technique of defects filling by using electrical field or current impulses that is not applicable for our study.

In order to obtain information about the deep levels of a semiconductor with PICTS, the thermal relaxation times τ_i must be calculated from the time dependence of the photoinduced current transient $I(t)$ [16–25]:

$$I(t) = I_0 + \sum_{i=1}^{n} \gamma_i \frac{e^{-t/\tau_i}}{\tau_i}, \quad (1)$$

where n is the number of distinct deep levels, I_0 denotes the dark current and the coefficient γ_i specifies the contribution of each level to the photoinduced current.

When the light excitation is switched off, the thermal emission of trapped carriers from the defects is governed by the physical process of thermal detrapping with a characteristic time constant that depends strongly on the temperature. The temperature dependence of the thermal relaxation times is inversely proportional to the emission rate e_t which is given by [16–25]:

$$e_t(T) = \frac{1}{g}\sigma_t v_{th} N_c exp(-E_t/kT) = \sigma_t T^2 B exp(-E_t/kT), \quad (2)$$

where g is degeneracy factor; v_{th} is thermal velocity; N_c is effective density of states in the conduction band; σ_t is the apparent capture cross–section of the trap levels; B is a temperature independent factor; E_t is the activation energy of the recharging defect, k is Boltzmann constant, and T is the absolute temperature. The quantity $v_{th}N_c$ varies as T^2, and thus, if e_t is measured as function of temperature, an Arrhenius plot e_t/T^2 vs. $1/T$ yields E_t (slope of Arrhenius plot) and σ_t (intercept at T^{-1}=0). The capture cross section calculated in such way is an apparent capture cross section because, in general, the electron and hole capture cross sections are temperature dependent.

Pulse-echo overlap method at megahertz range was used to study the elastic properties of $TlInS_2$ single crystals from ultrasonic velocity measurements at temperatures region 90–300 K. Our goal was to provide evidence of the possibility to make interconnection between deep trapping centers in $TlInS_2$ and ultrasonic measurements. For this purpose the changes of ultrasound velocity in unpoled and previously electro-poled $TlInS_2$ crystal (by application of an external electric field to $TlInS_2$ sample) were measured. A number of anomalies in the temperature dependence of ultrasound waves were determined for the first time in a complete compliance with PICTS-data.

The well-known feature of $TlInS_2$ crystals was taken into account in our considerations-the coexistence of ferroelectric and semiconductor properties. On cooling $TlInS_2$ displays the sequence of phase transitions from monoclinic paraelectric phase with space group symmetry C_{2h}^6 to incommensurate phase (INC) at T_i~216 K and commensurate improper ferroelectric phase at T_c~200 K. The INC-phase in $TlInS_2$ is the spatially modulated state with the modulation wave vector $\boldsymbol{k_i}=\delta(\boldsymbol{a}^* + \boldsymbol{b}^*)+0.25\boldsymbol{c}^*$, where $\delta \ll 1$ and $\boldsymbol{a}^*$, $\boldsymbol{b}^*$and $\boldsymbol{c}^*$ are reciprocal lattice vectors of the paraelectric phase. In the commensurate ferroelectric phase lock-in wave vector is k_c=0.25$\boldsymbol{c}^*$ with the spontaneous polarization directed along the crystallographic $\boldsymbol{b}$-axis. Obtained experimental results have made it possible to get deeper understanding of peculiarities of the phase transitions occurring in $TlInS_2$ crystals as well.

2. Experimental procedure

2.1. Sample preparation

The starting polycrystalline materials were synthesized from elements Tl, In and S of 5 N purity in conical quartz ampoules. The ampoules were charged with quantities of Tl, In and S in the ratio corresponding to the stoichiometry. The charged ampoules were then evacuated to a pressure of 10^{-5} Torr and sealed. The synthesis was carried out in a horizontal furnace at a temperature of 1033 K for 48 h.

$TlInS_2$ single crystals were grown by using the modified Bridgman method. Two different samples for PICTS and ultrasonic measurements were taken from the middle part of the ingots. Ingots were cleaved perpendicular to the $\boldsymbol{c}$–axis using a fine blade. The electrical resistivity of the ingot was measured to be around 5.7×10^9 Ω cm at room temperature.

The chemical composition of the synthesized crystals was determined by the energy dispersive spectroscopic analysis using a scanning electron microscope (SEM). The energy dispersive X-ray (EDX) analysis performed at room temperature confirmed that the content of the elements in the $TlInS_2$ crystal was coinciding well with the composition of the initial charge. For example, the atomic composition ratio of constituent elements Tl:In:S was found out as 25.12:24.07:49.59 at%, respectively. The SEM inspection also showed that $TlInS_2$ samples contained an insignificant percentage of background impurities, such as carbon, oxygen and silicon (with total concentration ~ 1.22 at%.).

2.2. PICTS–experimental setup

PICTS is used for studying defect levels in high-resistivity materials such as $TlInS_2$. To obtain information about the intrinsic deep levels in $TlInS_2$ crystal the photoinduced current transients are recorded between 77 and 350 K with a temperature step of ~1 K on heating regime.

$TlInS_2$ sample of $2 \times 4 \times 1$ mm^3 with a parallel contacts geometry was used. Both contacts were on the lateral sides of the sample and the region between the contacts was illuminated to produce the photoconductive response. The indium contacts were soldered to the lateral sides of the sample. The metallic contacts

were ohmic. The spacing between two indium electrodes was about 2 mm. The measuring circuit was typical for photocurrent investigation. A bias voltage of 50 V was applied across the sample contacts. Thus, in-layer-plane direction was used for the transient photocurrent measurements.

The registration of photo-current response decays was performed over the temperature range of 77–350 K. The sample was attached by means of an electrical insulating thermal conducting paste to the massive aluminum cold finger of the liquid nitrogen cryostat with a transparent entrance window. Hell-700 temperature sensor was attached to the sample holder near the sample for monitoring its temperature, and also connected to a temperature controller. A heater attached to the sample holder was enabled temperature control from 77 to 350 K using a programmable heating rate of 1 K/min. The measurement is based on the fact that during the light pulse, empty carrier traps are filled with generated photocarriers, leaving an increase in majority carrier concentration and resulting in an increase in conductivity. Thermally stimulated processes then cause the emission of the trapped minority carriers, which induces a decay of the photocurrent. Current transients were recorded at various temperatures and analyzed in a way similar to that used in deep level transient spectroscopy to obtain the trap release kinetics.

The illumination source was a xenon light beam passing through different 2.15–2.30 eV low-pass filters (bulk excitation). The measurements were performed under chopped illumination (asymmetrical square light pulses).

We use the sub-or near band-to-band gap excitation instead the band-to-band excitation, because photocurrent produced by band-to-band excitation persists for $TlInS_2$ crystals especially at low temperatures. In the background of the large photocurrent signals corresponding to band–to-band excitation, the thermal emission from deep level traps are not detectable and therefore the deep level defect characteristics cannot be founded. Thus, photoexcitation pulse corresponded to the maximum photoresponse was directed normal to the layer plane of $TlInS_2$ sample. The photon flux density was 10^{14} $cm^{-2}s^{-1}$ at the sample surface. The frequency of pulse excitation was equal to 20 Hz with light-to dark duration in the ratio of 1:5. The duration of excitation pulse was 30 ms.

The transient signal from the sample during the dark interval was captured at each selected temperature and processed online using data acquisition and control software. The photocurrent transients were normalized with respect to the photocurrent amplitude at the end of the light pulse. A home-made data acquisition system with preliminary processing and registration of transient data on a personal computer was used. Point wise accumulation and averaging were carried out across 64 realizations of photoresponse decay containing 2000 samplings located at a fixed time interval $\Delta t = 5 \times 10^{-5}$μs. Ferroelectric nature of the crystal was also taken into consideration. A conventional Deep Level Transient Spectroscopy technique was applied for the photoresponse transient analysis using a rectangular lock-in weighting function. The data registration allowed the characterization of relaxation times in the range of 0.5–37.7 ms with regard to the selected conditions. The activation energy (E_t) and the capture cross section (σ_t) of the intrinsic deep levels were calculated from the temperature dependence of the thermal relaxation times.

2.3. The measurements of ultrasound velocities

Ultrasonic pulse-echo overlap method is employed to measure the pulse transit times accurately, which is used to evaluate the mode velocity. The technical details of the pulse echo overlap method are discussed at length in literature [27–29]. An ultrasonic pulse passed through the sample is reflected from the opposite sample surface and comes back to the "sample-transducer" interface and is again reflected to the sample. Ultrasound pulses reflected as a result of multiple passages through the sample are inversely transformed by the same transducer to the electrical signal which are observed on the oscilloscope screen as a set of – pulse-echo reflections with amplitudes decreasing in time because ultrasound wave is absorbed by the sample.

By using pulse echo overlap technique, two successive ones of all pulse echo reflections are selected and overlapped by post signal process. Corresponding time τ of flight through the sample surfaces, between ultrasonic pulses is measured accurately. Ultrasound velocity v is determined from $v = 2d/\tau$, where d is sample length which is measured by using a micrometer in room temperature.

When the temperature is changed the overlapped echoes starts shifting of the oscilloscope screen. By the subunit electronics the echoes are again overlapped and the corresponding frequency is noted on a frequency counter for a particular temperature and hence the corresponding ultrasonic velocity. This procedure is repeated at different temperatures of interest. The accuracy in these measurements is better than 1% in the values of the longitudinal and better than 0.2% for shear ultrasonic waves, considering all sources of errors in the measurements.

In this paper the temperature dependence of the thermal emission rate is drawn and fitted with the Arrhenius formula for each of the deep level traps detected in $TlInS_2$.

The velocities of longitudinal and transverse ultrasonic waves in $TlInS_2$ were measured by means of the pulse-echo overlap method ranging for temperatures from 90 to 300 K. An automated and programmed pulse modulator and receiver electronic systems were used to identify the correct overlap of the echoes and to correct for the phase change introduced by the bonding medium on the ultrasonic pulses. A commercial type transducer having a diameter of 3 mm was used to send the ultrasonic waves through the solid $TlInS_2$ crystal. Longitudinal and shear type transducers have been employed to generate and detect ultrasonic waves of longitudinal and transverse polarizations. The transducer was mounted in a holder and held in place by fixing. The transducer was in the well mechanical contact with $TlInS_2$ samples surface. Apiezon N (Silicone) grease was found to be a suitable coupling agent to transmit ultrasonic wave pulses into the $TlInS_2$ sample at low temperatures. The fundamental frequency of the transducers was 10 MHz. The pulses were transmitted from the pulse receiver electronics to transducer.

The temperature was measured by means of diode sensor DT-670B attached to the holder near the sample. A resistive heater were mounted to holder and used to control the temperature with an accuracy of less than ~ 0.1 K by using a Lake Shore-338 auto tuning temperature controller. The submersible liquid nitrogen cryostat was used for the temperature conditioning at low temperatures.

After the system was evacuated until reaching of vacuum of the order of 10^{-1} mbar it was closed off with the atmosphere of gaseous nitrogen in it at room temperature. Liquid nitrogen was poured in the nitrogen Dewar and the bath level was raised until the copper sample holder was cooled to 90 K.

3. Experimental results

3.1. Characterization of traps

Fig. 1 shows the set of PICTS spectra of the high resistivity undoped $TlInS_2$ sample in the temperature range from 77 to 350 K corresponded to different characteristic relaxation times, where five major peaks labeled as TE2, BT23, B5, B7 and D0 are presented.

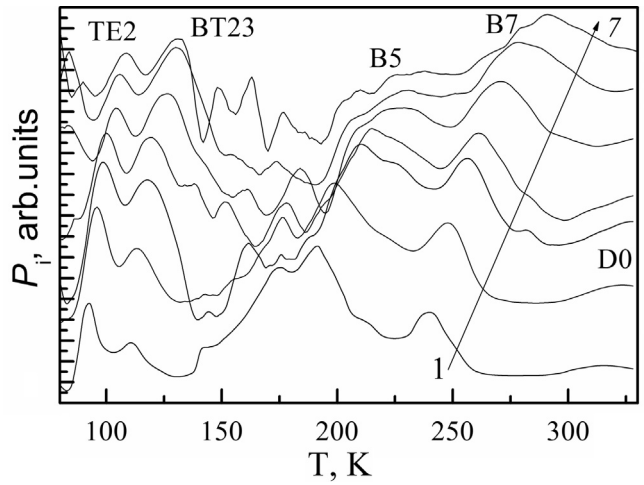

Fig. 1. PICTS spectra of $TlInS_2$ corresponding to the listed characteristic relaxation times; 37.7 ms, 17.8 ms, 7.0 ms, 4.1 ms, 1.8 ms, 0.9 ms, 0.5 ms. The spectra are normalized to the height of the maximal peak and shifted along *Y*-axis.

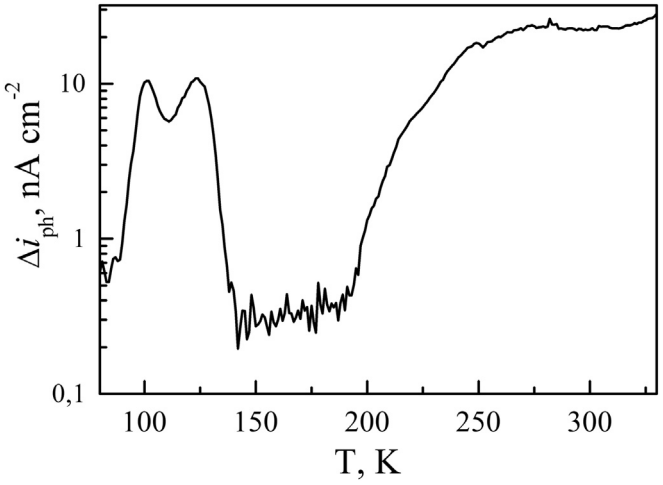

Fig. 2. Temperature dependence of photo-current response of $TlInS_2$ single crystals.

The PICTS technique does not determine the traps sign, i.e. it is a majority or minority carrier trap. To identify the level properly, one has to relate the PICTS results to other trap characterization methods. Since there is only ***p***-type $TlInS_2$ semiconductor we believe that TE2, BT23, B5, B7 and D0 are deep level acceptors. The deep level traps TE2, BT23, B5 and B7 were detected in Tb, Er, La and B doped $TlInS_2$ [11–15]. Therefore there are native structure defects of $TlInS_2$.

The change of crystal photo-current response with temperature is presented in Fig. 2. It can be noted that the signal of photo response is small in the temperature region between 145 and 185 K. As the consequence, the signal to noise ratio decreases and a spectra in this region contained less accurate data.

The Arrhenius plots (($ln(e_t/T^2)$ versus $10^3/T$)) of the five traps are shown in Fig. 3 and the resulting activation energy and the apparent capture cross section of all traps are reported in Table 1. While evaluating σ_t the effective mass of holes was taken 0.14 m_0 [30]. The error associated to the activation energy has been calculated from a chi-squared fitting procedure to each data set of the Arrhenius plot and resulted to be approximately 4%. Also, the temperature ranges ΔT for detected signals from traps are presented in the first column of the Table 1.

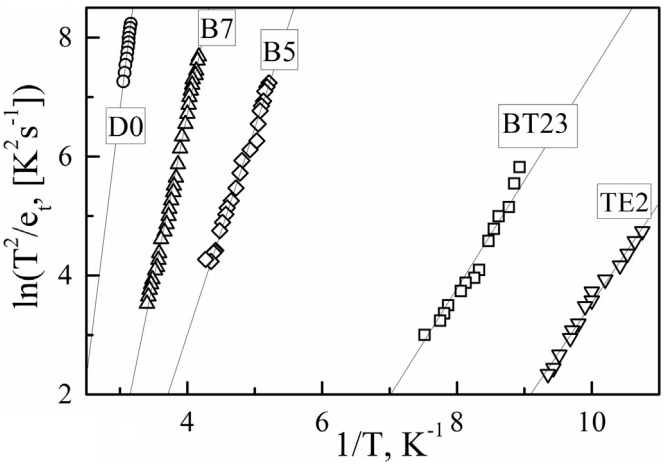

Fig. 3. Rate of charge carrier emission from deep level traps in $TlInS_2$ as function of temperature by taking into account T^2 correction. Solid lines represent the fitting to experimental data.

Table 1
Trapping parameters of $TlInS_2$ layered crystal.

	ΔT (K)	E_t (eV)	σ (cm^2)
TE2	93–110	0.16	6.9 10^{-15}
BT23	115–135	0.18	2.9 10^{-16}
B5	190–240	0.30	1.8 10^{-16}
B7	240–300	0.48	1.9 10^{-14}
D0	316–330	0.73	3.6 10^{-13}

The position of maximum corresponding to trap level B5 on the temperature scale of PICTS spectra corresponds to the temperature region of phase transitions in $TlInS_2$ [8–10,31,32]. The shift at the temperature position of the maximum in the set of spectra corresponding to various characteristic relaxation times is good when compared with the thermal activation of emission from the defects filled under photo excitation. It should be noted that it is not possible to determine the signs of the carriers trapped by centers (electrons or holes) in PICTS technique. We proposed that the detected defects are the traps of majority carriers since such trap centers are mostly observed in high-resistive semiconductors having a wide band gap [33,34].

Defects in undoped $TlInS_2$ crystals can be characterized by thermally stimulated current (TSC) spectroscopy, thermo-and photoluminescence [35–39]. These techniques were used to reveal information on various traps parameters (in a single temperature run) of $TlInS_2$ crystals such as the thermal activation energy, capture cross-section and concentration. The energy level and the emptied temperature of some traps in a TSC and thermo-and photoluminescence spectra of $TlInS_2$ are correlated with the appropriate dates revealed from PICTS measurements.

The interpretation of TSC spectra is complicated since measured TSC peaks are quite dependent on various measurement conditions (the heating rate, bias voltage, illumination time and delay time). According to this method traps are filled by a photo-excitation of semiconductors at low enough temperature such that upon ceasing the illumination, the trapped carrier cannot be freed by thermal energy available at that temperature. The temperature is then raised at a strictly constant rate. The liberated carriers contribute in an applied field, to an excess current until they recombine with carriers of opposite type. Due to its well resolved TSC spectra is observed in $TlInS_2$ semiconductors in which in addition to acceptor levels are donor impurity state too. Such

internally compensated $TlInS_2$ sample is very rarely to found in practice.

In addition, the measured TSC, thermo-and photoluminescence spectra of $TlInS_2$ were composed of many overlapping peaks [35,3]. The precise determination of trap levels in $TlInS_2$ by TSC, thermo-and photoluminescence measurements are difficult due to the mutual interference of overlapping peaks and their poor resolutions [35–39].

3.2. Temperature dependence of ultrasonic waves velocities in $TlInS_2$ crystals

In order to ascertain elastic modulus tensor components from the ultrasound velocity measurements for longitudinal and transverse acoustic waves propagating along the *c*-crystallographic axis in $TlInS_2$, we use equation [27–29]:

$$\rho v^2 S_i = C_{ijkl} n_j n_k S_l \tag{3}$$

where $i, j, k, l = 1,2,3$ and summation is carried out by twice repeating indices. All indices run over the range of the three cartesian coordinates. In (3), $\rho = 5.64 g/cm^3$ is the $TlInS_2$ crystal density, and v is ultrasonic wave velocity. The unit vector $\boldsymbol{n}$ is perpendicular to surface of constant phase or elastic wave front and determines the direction of ultrasonic wave propagation, and the unit vector $\boldsymbol{S}$ determines the polarization direction (i.e. direction of the displacement vector in elastic wave). C_{ijkl} is the moduli of elasticity.

As mentioned in Introduction, $TlInS_2$ crystal has the monoclinic structure (the space symmetry group is C_{2h}^6) at the indoor temperature. At that, $\boldsymbol{a}$ and $\boldsymbol{b}$ axes of the monoclinic cell lay in the layer plane, and $\boldsymbol{c}$ axis subtends a small angle relative to the direction of the normal to layers $\boldsymbol{c}^*$. Preparation of $TlInS_2$ layered crystal sample with the faces cut with the monoclinic angle to the crystal layer plane is a sophisticated technological problem.

Let's introduce an orthogonal coordinate system where $\boldsymbol{a} \| X$, $\boldsymbol{b} \| Y$, and $\boldsymbol{c}^* \perp$ to the crystal layer plane assuming that the monoclinic angle β is slightly deviated from the right angle. Using the equation of motion (3), we can write relations characterizing the velocity of ultrasonic wave propagating along the crystallographic axis $\boldsymbol{c}^* (n_1 = n_2 = 0;\ n_3 = 1)$. The velocity of transverse wave propagating along $\boldsymbol{c}^*$ axis with the displacement vector coinciding with the crystallographic axis $\boldsymbol{a}$ and $\boldsymbol{b}$ are respectively:

$$\rho v^2 = \frac{1}{2}(C_{33} + C_{55}) - \sqrt{\frac{(C_{33} + C_{55})}{2} + C_{35}^2}$$
$$and\ \rho v^2 = C_{44} \tag{4}$$

The velocity of longitudinal wave propagating along $\boldsymbol{c}^*$ axis and polarized in the same direction is:

$$\rho v^2 = \frac{1}{2}(C_{33} + C_{55}) + \sqrt{\frac{(C_{33} - C_{55})}{2} + C_{35}^2} \tag{5}$$

As it is known, layered crystal structure of $TlInS_2$ can be interpreted as quasi-tetragonal because many physical properties do not exhibit anisotropy in the plane of the layer [31,32]. Taking into account this assumption and assuming that for tetragonal crystals $C_{44} = C_{55}$ and C_{35}=0 [40], we can make the conclusions about ultrasound waves propagating perpendicular to layer of $TlInS_2$ as follows: the velocity of longitudinal wave propagating along the $\boldsymbol{c}^*$ axes and polarized in the same direction is determined by the elastic constant C_{33}; the velocity of transverse wave propagating along the $\boldsymbol{c}^*$ axes with the displacement vector laying in the in the crystal layer plane is determined by the shear constant C_{44}.

The velocity change of longitudinal ultrasonic waves propagating in the direction perpendicular to the layers plane

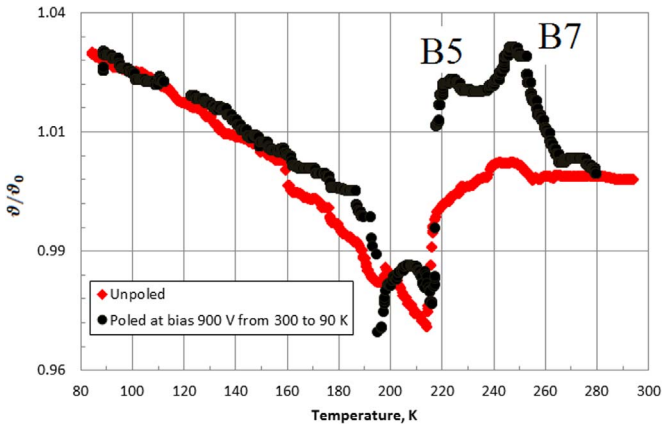

Fig. 4. The temperature variation of the velocity of longitudinal ultrasonic wave propagating along the [001] direction.

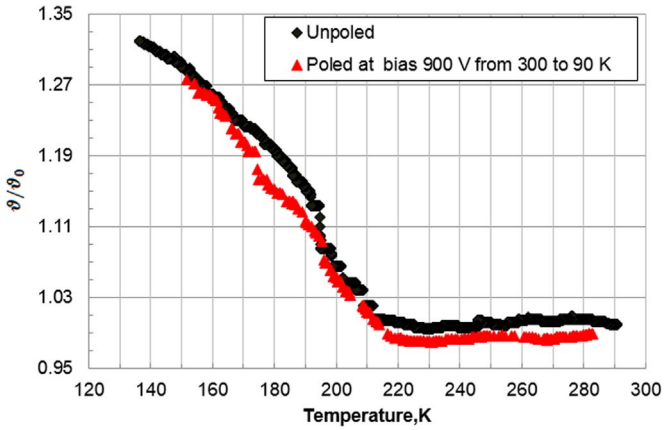

Fig. 5. The temperature variation of the velocity of transverse ultrasonic wave propagating along the [001] direction.

determined by the elastic constant C_{33} was shown in Fig. 4. It implies that the temperature dependence of longitudinal ultrasonic velocity is subject to significant changes in the vicinity of the phase transition to the INC-phase: this elastic mode velocity decreases sharply in the vicinity of $T_i = 210$ K, passes through the minimum and then increases with a positive temperature slope. It is typical of velocity anomaly for this wave in $TlInS_2$ [31]. The value of jump in behavior of elastic mode velocity is equal to ~6% on average.

A small break in behavior of this acoustic mode is observed at T_c~196 K [31]. Anomalous behavior of this elastic mode indicates that $TlInS_2$ crystal lattice is elastically "softened" in the vicinity of the phase transitions. As the temperature decreases down below T_c the elastic constant C_{33} increases with a slight shift from linearity.

Fig. 5 shows the temperature behaviour of transverse acoustic wave propagating perpendicular to layers with the displacement vector parallel to the layer plane. The temperature behavior of velocity of this elastic mode is determined by the shear constant C_{44}. As evident from Fig. 5, the temperature dependence of this wave velocity $(C_{44}(T))$ has an unusual character in the temperature range under consideration. As the temperature decreases starting from the ~300 K the velocity of transverse ultrasonic wave under study decreases already in the paraelectric phase of $TlInS_2$ crystal [31]. From Fig. 5 one can see also that temperature dependence of transverse ultrasonic wave velocity corresponding to shear constant C_{44} changes its slope at T_i. Small anomaly was observed out in behavior of this wave velocity in the vicinity of T_c in $TlInS_2$.

3.3. Temperature dependence of ultrasonic velocities in electro-polled $TlInS_2$ crystal

Electro-poling of $TlInS_2$ is based on the application of an external electric field to a sample at different temperatures. During the poling process, the $TlInS_2$ sample was submitted to a static external electric field. The electric field can be generated by the simple application of an electrical potential drop for an extended period of time via two electrodes that are fixed to either side of the $TlInS_2$ sample. The sample was previously cooled from 300 down to 90 K under bias electric field ~3 kV/cm applied along the layers plane.

Fig. 4 displays the temperature dependence of the longitudinal ultrasonic wave velocity determined by the elastic constant C_{33} recorded directly after crystal electro–poling with heating rate ~ 1 K/min. It can be seen that two maxima located in temperature region above T_i are revealed after the electro-poling. The anomalous behavior observed in the sound velocity in the temperature region $T>T_i$ for polled sample is unique in nature. It is important to note that the locations of these maxima are correlated with the area of thermal activation of B5 and B7 deep level traps revealed from PICTS measurements.

The temperature dependence of the transverse ultrasonic wave velocity determined by the shear elastic constant C_{44} recorded directly after crystal electro-poling with heating rate ~ 1 K/min is given in Fig. 5. No substantial changes are registered.

4. Discussion

The main question needing explanation is: how an effective local potential for any charged deep level or some electrostatic dipole in bulk of $TlInS_2$ can affect lattice structure of polled crystal. It is clear that the inverse piezoelectric effect may be responsible for this effect. The velocity of sound depends on a stress distribution in materials. Generally stress distribution inside the materials is continuous. It is quite clear that local potential of charged defect can significantly affect the stress distribution pattern within the lattice. When the acoustic wave front reaches the region of active defects network, the material properties related with the propagation of ultrasonic wave change by the internal stress distributions near the defects. Therefore, the velocity of sound in $TlInS_2$ can be controlled by native deep defects. The new strain distribution within the lattice induced by bias voltage applied to the crystal is favorable mechanism for the answer to the above question. We consider this idea in more detail below.

When electrostatic electrical field is applied, the corresponding change in the polarization of medium results in an extra deformation, termed inverse piezoelectric effect [41,42]. Let's suppose that $TlInS_2$ is polled parallel to the x-axis ($x \| \boldsymbol{a}$-crystal axis). Then, the dipole moments of polarized deep level defects are directed along the x-axis. Let P_x denotes the crystal polarization along the x-axis. Then, we have the following matrix equation for tetragonal crystal structure [41,42]:

$$\begin{pmatrix} P_x^x \\ P_x^y \\ P_x^z \end{pmatrix} = \begin{pmatrix} d_{11} & d_{12} & d_{13} & 0 & 0 & 0 \\ 0 & 0 & 0 & 0 & 0 & d_{16} \\ 0 & 0 & 0 & 0 & d_{15} & 0 \end{pmatrix} \begin{pmatrix} u_{xx} \\ u_{yy} \\ u_{zz} \\ u_{yz} \\ u_{xz} \\ u_{xy} \end{pmatrix} \quad (6)$$

Here d_{ij} and u_{ij} are inverse piezoelectric polarization coefficients and strain components along the respective axes, respectively. As an example, P_x^ymeans the polarization along x-axis producing the u_{yy} component of strain tensor. From the Eq. (6) we have:

$$P_x^x = 2d_{11}u_{xx} + d_{13}u_{zz} \quad (7)$$

For simplicity, we assume in (7) that $d_{11} = d_{12}$ and $u_{xx} = u_{yy}$. This presumption is based on the fact that $TlInS_2$ layered crystal doesn't exhibit any observable anisotropy in the layers plane.

First, it is clear from (7) that there is no interconnection between P_x^x and share deformations u_{xz} and/or u_{yz}, that is why the electro–poling of the crystal applying the electric field along the layers plane affects the temperature dependence of the longitudinal ultrasonic wave velocity and does not affect the transverse one.

Second important result from comparison of (7) and experimental data is that d_{13} is not negligible comparing with d_{11}, although such a result seems to be quite predictable for crystal with layered structure. As it was mentioned in a number of our previous investigations [27,43,44], crystals from $TlInS_2$ family often demonstrate the "unusual" strong coupling between interlayer and intralayer deformations. We can propose now that such "unusual" behavior can be due to native charged defects which play an important role in almost all physical properties in $TlInS_2$ type crystals.

5. Conclusions

In summary, we have investigated the deep energy levels induced by native defects in $TlInS_2$ layered semiconductor by PICTS technique. Five major native traps was revealed in the $TlInS_2$ ternary compound. Using the pulse-echo overlap method, the speed of the longitudinal and transverse sound waves propagating in $\boldsymbol{c}$-crystallographic directions of $TlInS_2$ were measured before and after electro-poling $TlInS_2$ in an external electric field applied along the crystal plane. Two deep levels B5 and B7 with energy 0.30 eV and 0.48 eV are responsible for the modification of longitudinal ultrasonic mode velocity in the temperature range where these defects are active for electro-polled $TlInS_2$. A phenomenological model based on the inverse piezoelectric effect was proposed to account qualitatively for the experimental observations. According to this model, the built-in an internal electric field originated from the poling of the crystal in the layers plane induces the large u_{zz} intrinsic lattice strain in the temperature range where defects are active. This result explains previous experimental observations of "strange" coupling between interlayer and intralayer deformations in the crystals of $TlInS_2$ family.

References

[1] W. Henkel, H.D. Hochheimer, C. Carlone, A. Werner, S. Ves, H.G. Vonschnering, Phys. Rev. B 26 (1982) 3211.
[2] B.I. Shklovskii, A.L. Efros, Sov. Phys. JETP 35 (1972) 610.
[3] M. Isik, S. Delice, N.M. Gasanly, Acta Phys. Pol. A 126 (2014) 1299.
[4] N.S. Yuksek, N.M. Gasanly, H. Ozkan, O. Karci, Acta Phys. Pol. A 106 (2004) 95.
[5] S. Özdemir, R.A. Suleymanov, E. Civan, T. Firat, Solid State Commun. 98 (1996) 385.
[6] M. Isik, N.M. Gasanly, H. Ozkan, Acta Phys. Pol. A 115 (2009) 732.
[7] S. Ozdemir, M. Bucurgat, Curr. Appl. Phys. 13 (2013) 1948.
[8] K.R. Allakhverdiev, N.D. Akhmed-zade, T.G. Mamedov, T.S. Mamedov, M. Yu Seidov, Low. Temp. Phys. 26 (2000) 56.
[9] M. Yu Seyidov, R.A. Suleymanov, S.S. Babayev, T.G. Mammadov, A.I. Nadjafov, G.M. Sharifov, Phys. Solid State 51 (2009) 264.
[10] M. Yu Seyidov, R.A. Suleymanov, S.S. Babaev, T.G. Mammadov, G.M. Sharifov, Phys. Solid State 51 (2009) 568.
[11] M. Yu Seyidov, R.A. Suleymanov, A.P. Odrinskii, A.I. Nadjafov, T.G. Mammadov, E.G. Samadli, Jpn. J. Appl. Phys. 50 (2011) 05FC08.
[12] M. Yu Seyidov, R.A. Suleymanov, F.A. Mikailzade, E. Orhan Kargın, A. P. Odrinsky, J. Appl. Phys. 117 (2015) 224104.
[13] M.-H. Yu Seyidov, A.P. Odrinsky, R.A. Suleymanov, E. Acar, T.G. Mammadov, V. B. Alieva, Phys. Solid State 56 (2014) 2028.
[14] A.P. Odrinskii, T.G. Mamedov, M.-H. Yu Seyidov, V.B. Alieva, Phys. Solid State 56 (2014) 1605.
[15] M. Yu Seyidov, R.A. Suleymanov, E. Acar, A.P. Odrinsky, T.G. Mammadov, A.

I. Nadjafov, V.B. Aliyeva, Low. Temp. Phys. 40 (2014) 830.
[16] (a) J.C. Balland, J.P. Zielinger, C. Noguet, M. Tapiero, J. Phys. D: Appl. Phys. 19 (1986) 57;
(b) J. Phys. D: Appl. Phys. 19 (1986) 71.
[17] J.P. Zielinger, B. Pohoryles, J.C. Balland, J.G. Gross, A. Coret, J. Appl. Phys. 57 (1985) 293.
[18] S.D. Brotherton, J. Appl. Phys. 55 (1984) 3636.
[19] Yutaka Tokuda, Akira Usami, Yajiro Inoue, Semicond. Sci. Technol. 2 (1987) 251.
[20] (a) O. Yoshie, M. Kamihara, Jpn. J. Appl. Phys. 22 (1983) 621;
(b) Jpn. J. Appl. Phys. 22 (1983) 629;
(c) Jpn. J. Appl. Phys. 24 (1985) 431.
[21] A. Blondeel, P. Clauws, J. Appl. Phys. 86 (1999) 940.
[22] M. Yu Seyidov, F.A. Mikailzade, T. Uzun, A.P. Odrinsky, E. Yakar, V.B. Aliyeva, S. S. Babayev, T.G. Mammado, Physica B. 483 (2016) 82.
[23] P. Blood, J.W. Orton, The Electrical Characterizations of Semiconductors: Majority Carriers an Electron States, Academic Press, London, UK, 1992.
[24] D.V. Lang, J. Appl. Phys. 45 (1974) 3023.
[25] Ch Hurter, M. Boilou, A. Mitonneau, D. Bois, Appl. Phys. Lett. 32 (1978) 821.
[26] J.S. Laird, C. Jagadish, D.N. Jamieson, G.J.F. Legge, J. Phys. D: Appl. Phys. 39 (2006) 1342–1352.
[27] B. Luthi, Physical Acoustics in the Solid State, Springer, Berlin, Heidelberg, New York, 2005.
[28] D. Royer, E. Dieulesaint, D.P. Morgan, Elastic Waves in Solids, 1,2, Springer, Berlin, Heidelberg, New York, 2000.
[29] R. Truell, C. Elbaum, B.B. Chik, Ultrasonic Methods in Solid State Physics, Academic Press, New York and London, 1969.
[30] A.F. Qasrawi, N.M. Gasanly, Mater. Res. Bull. 39 (2004) 1353.
[31] Yu.V. Ilisavskii, V.M. Sternin, R.A. Suleimanov, M. Yu Seyidov, F.M. Salaev, Sov. Phys. -Solid State 33 (1991) 104.
[32] R.A. Suleimanov, M. Yu Seidov, F.M. Salaev, Sov. Phys. -Solid State 33 (1991) 1797.
[33] J.W. Farmer, C.D. Lamp, J.M. Meese, Appl. Phys. Lett. 41 (1982) 1063.
[34] A.G. Milnes, Deep Impurites in Semiconductors, John Wiley & Sons, New York, London, Sydney, Toronto, 1973.
[35] M. Isik, S. Delice, N.M. Gasanly, Acta Phys. Pol. A 126 (2014) 1299.
[36] A.F. Qasrawi, N.M. Gasanly, Phys. Status Solidi A 199 (2003) 277.
[37] M. Isik, N.M. Gasanly, H. Ozkan, Acta Phys. Pol. A 115 (2009) 732.
[38] S. Ozdemir, R.A. Suleymanov, E. Civan, T. Firat, Solid State Comm. 98 (1996) 385.
[39] S. Ozdemir, M. Bucurgat, Curr. Appl. Phys. 13 (2013) 1948.
[40] J.F. Nye, Physical Properties of Crystals. Their Representation by Tensors and Matrices, Oxford University Press, 2006.
[41] B.A. Strukov, A.P. Levanyuk, Ferroelectric Phenomena in Crystals, Springer, Berlin, Heidelberg, New York, 1998.
[42] J. Yang, An Introduction to the Theory of Piezoelectricity, Springer, Boston, 2004.
[43] M. Yu Seyidov, R.A. Suleymanov, J. Appl. Phys. 108 (2010) 063540.
[44] G.L. Belenkii, E. Yu Salaev, R.A. Suleimanov, Sov. Phys. Uspekhi 31 (1988) 433.